Catalysis Today 202 (2013) 197–209

Contents lists available at SciVerse ScienceDirect

Catalysis Today

journal homepage: www.elsevier.com/locate/cattod

Electrocatalysis: A direct alcohol fuel cell and surface science perspective

B. Braunchweig[a], D. Hibbitts[b], M. Neurock[b], A. Wieckowski[a,*]

[a] Department of Chemistry, University of Illinois at Urbana-Champaign, Urbana, IL 61801, United States
[b] Departments of Chemical Engineering and Chemistry, University of Virginia, Charlottesville, VA 22904-4741, United States

ARTICLE INFO

Article history:
Received 20 February 2012
Received in revised form 19 June 2012
Accepted 10 August 2012
Available online 9 October 2012

Keywords:
Electrocatalysis
Methanol
Ethanol
Fuel cells
Sum frequency generation
DFT theory

ABSTRACT

In this report, we discuss some of the advances in surface science and theory that have enabled a more detailed understanding of the mechanisms that govern the electrocatalysis. More specifically, we examine in detail the electrooxidation of C_1 and C_2 alcohol molecules in both acidic and basic media. A combination of detailed in situ spectroscopic measurements along with density functional theory calculations have helped to establish the mechanisms that control the reaction paths and the influence of acidic and alkaline media. We discuss some of the synergies and differences between electrocatalysis and aqueous phase heterogeneous catalysis. Such analyses begin to establish a common language and framework by which to compare as well as advance both fields.

1. Introduction

The rates of electrocatalytic reactions depend upon the surface structure and composition [1] of the electrode as well as on the applied potential [2]. The former includes the chemical composition of the electrode surface, its long-range geometry (with possible surface reconstructions or relaxations) and the in situ surface atomic arrangement on a short range scale whereas the later follows the changes that result in the atomic of the above as well as the electronic structure of the metal. Recent developments in electrocatalysis have been driven by progress in ab initio theory of catalysis, [4] development of new experiment methods to study materials and surfaces [6–8] and the synthesis of new catalytic materials [9–12]. The discovery of new nanoscale materials with unique surface structures and geometric architectures [9–11,13] often provide unexpected surface properties as well as enhanced electrocatalytic performance. Such structure–property relationships can be explored in detail through the use of in situ spectroscopy, rigorous materials characterization as well as by the use of first-principles quantum mechanical calculations and molecular simulations. This process of synergistically integrating detailed characterization and spectroscopy, theory, electrocatalytic performance and novel materials development provides consistency to the electrocatalysis field across its known efforts and domains.

The tremendous surge in the research efforts in modern electrocatalysis that have occurred over the past two decades have provided unprecedented advances in the fundamental principles that control electrocatalytic reactions and applications in fuel cell science where chemical energy stored in materials such as primary alcohols (methanol and ethanol), polyols (glycerol), and formic acid can be electrochemically converted in electricity. This has been led by the tremendous advances that have occurred in development and application of novel in situ spectroscopic methods, atomic-scale characterization techniques, and theory and simulation methods that provide a more detail molecular level insights in the factors that control electrocatalysis.

While the explosion of efforts focused on the application of fuel cells is impressive, there are a range of other exciting areas that have taken advantage of these fundamental efforts, including CO_2 reduction [14], electrochemical supercapacitors [15,16], and molecular electronics [17,18]. Another fast growing area are the generation of fuel for electrochemical applications from renewable resources and the design of efficient and selective catalysts for reactions that convert electrical energy into chemical bonds in fuels [19,20]. Beside research activities in the field of electrochemical energy generation, research for efficient energy storage e.g. for lithium ion batteries remains a highly active and growing field that does not show evidence of slowing down [21,22].

In general, a fuel cell is an electrochemical device [23] which requires electrocatalysts at the anode oxidize the fuel to produce electrons and protons and at the cathode reduce oxygen and consume the protons and electrons produced (as shown in Fig. 1). The differences in the rates of reaction at the anode and cathode

* Corresponding author.
E-mail address: andrzej@scs.uiuc.edu (A. Wieckowski).

0920-5861/$ – see front matter © 2012 Elsevier B.V. All rights reserved.
http://dx.doi.org/10.1016/j.cattod.2012.08.013

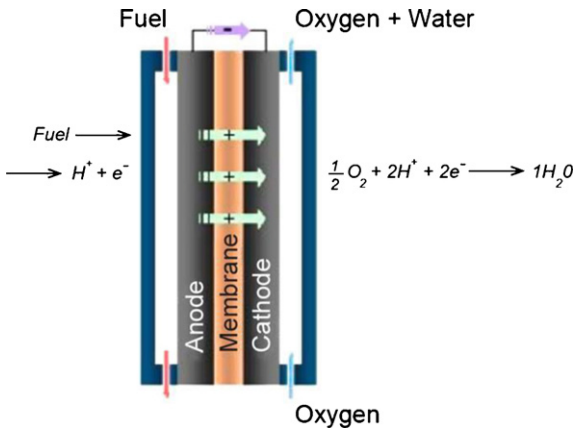

Fig. 1. A schematic of the polymer fuel cell. The proton conducting membrane, such as Nafion allows the proton to rapidly transfer from the anode to the cathode whereas the wire which connects the two electrodes allows for electron transfer. The fuel oxidation at the anode and the reduction of oxygen which occurs at the cathode are shown.

Source: www-rpl.stanford.edu.

dictate the potential at which the cell can operate and the maximum current density. On the anode side, the challenge is to efficiently catalyze the oxidation of hydrogen or oxygenate fuels such as methanol, formic acid or ethanol. Unfortunately, the fuel sources are often contaminated by CO or other species that can poison the electrode surface. On the cathode side, the requirement is to effectively reduce oxygen [24], usually from air and to prevent the dissolution and loss of catalyst. The most active electrocatalytic materials are typically comprised of expensive transition metals nanoparticles such as Pt that are too costly to provide viable commercial solutions. Core–shell [25] nanoparticles have of a very thin shell of the active Pt catalyst supported onto a second metal. To synthesize these systems, bimetallic nanoparticles are often leached in acid to remove the excess of the electro-dissolving non-noble element leaving the protective layer composed of the Pt or the Pt-enriched surface phase [25]. In other words, the electro-dissolution creates de-alloyed Pt bimetallic catalysts that are composed of an inexpensive core element with platinum present only in the nanoparticle shell. This leaves the composition of the material in use active and close to the nominal (started) alloyed/bimetallic specification.

Dissolution also results in lattice mismatch between the core and the shell [26] that may lead to enhanced activity (d-band rearrangement of the bimetallic catalyst causes weakens chemisorption of oxygen to improve the catalytic rate of the oxygen reduction reaction, ORR [24]). Most frequently, dealloyed Pt–Co bimetallic alloy nanoparticles are studied for electrocatalyst cathodes [27,28].

The primary challenge at both the anode as well as the cathode is to maintain the catalyst activity for at least a few thousand hours. Despite the significant academic and industrial research and development efforts, electrocatalytic materials are still quite a ways away from meeting these requirements and thus requiring more dedicated research efforts. In addition, while recent efforts have helped to reduce the amount of platinum required at the anode for neat hydrogen applications, there are still significant challenges in reducing the amount of Pt at the anode for more the oxidation of hydrogen reformate (containing a measurable amount of CO) thus creating further research needs. The use of ruthenium additives to platinum to promote CO oxidation at the anode offers one solution that will be discussed later in this paper.

Significant developments in the application of electrochemical devices and the design of new electrocatalytic materials have been significantly advanced by the developments and application of detailed materials characterization and surface science. The understanding of the surface structure and composition of the active catalytic materials, the nature of the active site, and insights into the interaction between three-phase interface that occurs between the metal, polymer electrolyte and the carbon-conducting support have been advanced by the applications of surface sensitive probes, such as synchrotron extended X-ray absorption spectroscopy (EXAFS) and the synchrotron X-ray absorption near edge spectroscopy (XANES), electron microscopy (TEM), Auger electron spectroscopy (AES), X-ray photoelectron spectroscopy (XPS) and UV photoelectron spectroscopy (UPS), just to mention a few. Except for the synchrotron options, the procedure requires bringing the electrode from an electrochemical cell to an ultra-high vacuum (UHV) for a post-pumping electrode characterization. Fortunately, pumping is not breaking chemical bonds in stable electrode systems [29], so genuine information on the electrode adsorption state (in solution) is obtained through the measurements in UHV [30]. Such an "emersion" experiment connects electrode adsorption study and study of adsorption in UHV the most directly. However, water desorbs to UHV from metal surfaces at ca. 160 K which may destabilize some of the electrode systems.

2. Surface vibrational spectroscopy with SFG in fuel cell electrocatalysis

Ethanol is an interesting feed for fuel cells [31–33] that can be produced from biomass. It is renewable, and its complete oxidation to CO_2 provides a comparably high yield of twelve electrons per molecule [34]. While fuel cell reactions involving ethanol have been intensively investigated and reported [35–45], new observations were provided by in situ, Fourier transformed, infrared spectroscopy (FTIR) [46,47] and broad-band sum-frequency spectroscopy (BB-SFG). Using an attenuated and surface enhanced FTIR (ATR-FTIRS) it was shown that the catalytic oxidation of ethanol on polycrystalline Pt leads to predominant formation of acetaldehyde and acetyl [46,47] intermediates on the electrode surface that can subsequently decompose to form CO which at lower potentials poisons the surface.

SFG is a powerful vibrational spectroscopic technique for studies of surfaces and interfaces [48,49]. The sum-frequency is generated by overlapping a tunable infrared and a fixed visible laser beam in time and space at the interface of interest. The SFG intensity is proportional to the square of the second-order susceptibility $\chi^{(2)}$ [49], which vanishes within the dipole approximation in the bulk of centrosymmetric materials such as platinum and aqueous electrolytes. Surfaces and interfaces, however, necessarily break the prevailing centrosymmetry and give rise to non-vanishing $\chi^{(2)}$ contributions from the interface. For that reason SFG signals from the bulk of centrosymmetric materials are virtually absent and molecular layer on electrode surface such as adsorbed CO, but also a number of other adsorbed molecules become accessible with SFG [31,50].

The following equation describes the model used for the intensity $I(\omega_{SF})$ of the SFG signals and its dependent parameters:

$$I(\omega_{SF}) \propto \left|\chi^{(2)}_{NR} + \sum_q \chi^{(2)}_q\right| \left|I(\omega_{vis})I(\omega_{IR}) \cdot \exp\left[-4\ln 2\frac{(\omega_{IR}-\Omega)}{\Delta^2}\right]\right.$$

$$\text{with} \quad \chi^{(2)}_q = \frac{A_q e^{i\theta_q}}{(\omega_q - \omega_{IR} + i\Gamma_q)}$$

Here, $\chi^{(2)}_{NR}$ and $\chi^{(2)}_q$ correspond to the non-resonant and resonant parts of $\chi^{(2)}$, respectively. The resonant part of $\chi^{(2)}$ is related to the amplitude A_q, frequency ω_q, bandwidth Γ_q and phase θ_q of the qth vibrational mode, while $\chi^{(2)}_{NR}$ is due to non-resonant electronic excitations at the interface. In broadband SFG (BB-SFG) a

tunable broadband infrared (BBIR) laser pulses with the frequency Ω and a bandwidth Δ of >150 cm^{-1} are mixed at the interface with a narrowband (<10 cm^{-1}) 'visible' laser pulse, where the corresponding sum frequency of visible and IR frequencies is generated. Using BB-SFG, vibrational spectra can be recorded within the entire bandwidth of the BBIR pulse, which eliminates the need for tuning the IR frequency within the limit of the BBIR bandwidth and allows for rapid acquisitions of vibrational spectra [51,52].

Because we are mostly interested in the resonant contributions of $\chi^{(2)}$which are associated with adsorbed molecular species, we have applied a previously reported suppression technique [53,54] for the non-resonant contribution [50–56]. This technique, however, requires a compromise between a complete suppression of $\chi^{(2)}_{NR}$ and maintaining a relatively good signal-to-noise ratio of the observed vibrational bands. A detailed description of the BB-SFG setup can found elsewhere [54].

SFG helps to solve two of the greatest problems in surface molecular spectroscopy, sensitivity and selectivity. As described above selectivity results from being nonlinear and coherent while sensitivity is due to the product of IR and visible intensities at the surface, and the particularly huge intensity of focused femtosecond IR pulses.

The broadband-SFG (BB-SFG) apparatus for spectro-electrochemistry employed in this study is presented in Fig. 2. The spectrometer allows for rapid acquisitions of vibrational spectra synchronized with a voltammetric scan and has been reported elsewhere [51]. The broadband technique measures a spectrum with point-by-point scanning and obtains a large region of the SFG spectrum with every laser shot. As a result of high sensitivity, we can tolerate substantial IR attenuation due to the optical absorption of the aqueous electrolyte layer. We are able to use electrochemical cells where thickness of the electrolyte film is controlled by a spacer of thickness 25 μm or more [51]. The importance of using this thicker electrolyte cannot be overemphasized. Thinner electrolyte layers can significantly distort the electrochemistry and may lead to major errors in the interpretation of surface vibrational spectra. Too thin layers also preclude studies of fast kinetics due to the limited diffusion of reaction educts and product through the thin-layers electrolyte.

3. Advances in theory in electrocatalysis

The past decade has witnessed novel developments in ab initio methods and exponential advances in the computing power that have enabled the simulation of complex metal/solution interfaces and electrocatalytic systems. Anderson and colleagues [57–59] were some of the first to establish ab initio methods to treat electrochemical systems in their development of a reaction center model. While the reaction models were comprised of only one or two Pt atom centers, their results provided important insights into electrocatalytic behavior. Schmickler et al. [60,61] developed a model Hamiltonian that was subsequently used to capture bond-breaking and bond-making phenomena in electrochemical systems and provide novel insights in surface reaction chemistry. Nørskov and colleagues [62] developed and elegant approach in which gas phase surface energies can be used to predict the chemistry in the presence of solution and an applied surface potential. The approach is used by many today to provide a first-order understanding of the influence of potential.

These simple models were subsequently followed by more advanced methods and detailed simulations aimed at modeling the explicit factors that give rise to electrochemistry and electrocatalysis on metal surfaces at applied potentials. Filhol, Taylor and Neurock [63,64] used explicit electrolyte in solution along with the metal surface to examine the changes the result from an applied potential. The model was subsequently simplified by appropriately charging the metal and allowing for a counter charge in the aqueous media to establish the double layer at the interfaces. By using a double reference they could directly and quantitatively relate the changes in charge to the change in potential and thus control the potential at the interface. Otani et al. [65] coupled rigorous density functional theory methods to describe the chemistry at the metal surface together with an effective screening medium to mimic the polarizable continuum. Jinnouchi and Anderson [66] followed a similar approach but coupled DFT with a modified Poisson–Boltzmann theory to model the double layer. A more recent approach by Rossmeisl et al. [67] used explicit protons to simulate constant potential electrochemistry. All four of these methods offer unique insights into the interfacial electrochemistry

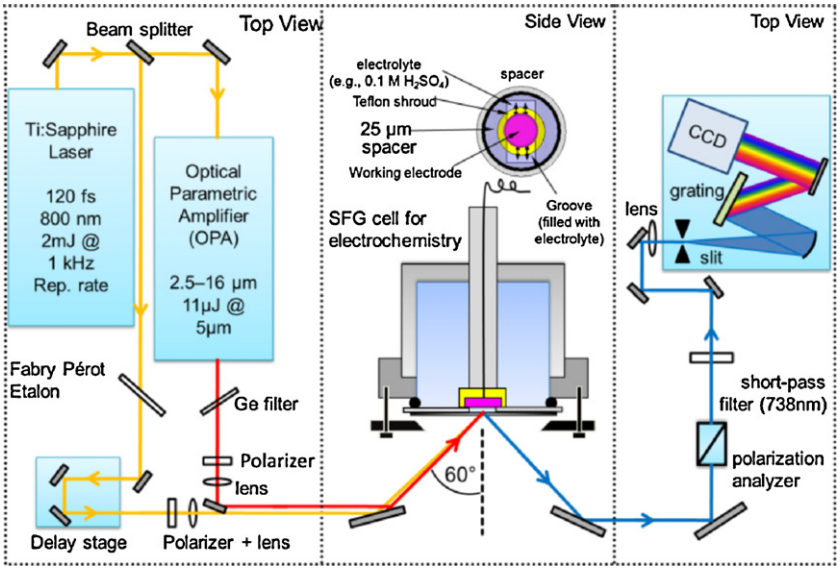

Fig. 2. Schematic setup for surface vibrational spectroscopy with broadband SFG synchronized with voltammetry. Top views show the necessary optics of the BB-SFG spectrometer, while the side view shows the basic components for simultaneous electrochemical characterizations.

but differ somewhat in the way in which they simulate the double layer.

4. Methanol electrocatalysis

The oxidation of methanol proceeds over most transition metals through a sequence of elementary C—H and O—H bond activation steps that occur on vacant surface sites on the metal, and ultimately result in the formation of CO [3]. Through the combination of cyclic voltammetry, chronoamperometry and DFT studies we confirmed that methanol decomposition occurs via a dual path mechanism [3]. At potentials below 0.35 V RHE, the mechanism proceeds predominantly through a sequence of C—H activation steps that lead to the formation of the hydroxyl methylene (CHOH) intermediate which subsequently reacts to form adsorbed CO. At potentials above 0.35 V, the O—H bond of methanol can also be activated thus resulting in the formation of formaldehyde which subsequently desorbs or continues to react to form CO. The onset potential was found to be a function of specific surface structure. The dual paths for the oxidation of methanol to CO over Pt(1 1 1) along with their corresponding reaction energies calculated at 0.5 V RHE are shown in Fig. 3. Stepped defect sites, which are known to be present on the Pt(1 1 1) surface, reduce the onset potential to 0.4 V which is consistent with the experimental results which indicate a value of 0.35 V RHE [3]. While CO is an intermediate to CO_2, it readily builds up on the surface at lower potentials and poisons more active metals such as Pt.

As stated, at higher potentials, the O—H bond of methanol can be activated on the Pt surface, leading to formation of formaldehyde. Formaldehyde can subsequently hydrate in solution to form methanediol via an equilibrium process [68]. Methanediol can subsequently dehydrogenate to form observed formic acid in solution, which can dissociatively adsorb on Pt resulting in adsorbed formate. Formate has been observed experimentally [69], and has been proposed as an active intermediate in the direct formation of CO_2 which proceeds via the C—H bond activation providing a path that bypasses the formation of the strongly bound CO intermediate. DFT calculations indicate that formate binds very strongly through the oxygen atoms in a di-sigma interaction. This binding mode will likely cause a large barrier for the final dehydrogenation of formate to form CO_2, which could explain why large overpotentials are required to fully oxidize the formate intermediate [69,70].

5. Methanol electrocatalysis on platinum surfaces containing ruthenium

Pt is often alloyed with a more oxophilic metal such as Ru to promote the adsorption and dissociation of water thus creating bifunctional sites on the surface [71–78]. These bifunctional fuel cell catalysts show enhanced "CO-tolerance" compared to pure Pt during methanol oxidation reactions [79]. Alloying Pt with Ru results in the formation of OH groups which interrupt the CO adlayer and readily oxidize CO to CO_2 (bifunctional effect) and in addition reduce the Pt–CO bond strength via an increased electron density on Pt through electronic interactions with Ru (ligand effect as per the NMR work: [80–82]). We also showed that CO adsorbed on nanoparticle Pt/Ru is confined within the Pt and Ru island borders on the surface [83]. The total effect of Ru is a reduction in the overpotential for CO oxidation by ~0.25 V [84–87] which leads to a decrease in CO poisoning during methanol oxidation.

6. Ethanol electrocatalysis

The electrocatalytic oxidation of ethanol is much more complex than the oxidation of C_1 molecules such as methanol or formic acid. The desired complete oxidation to CO_2 produces twelve electrons per molecule, which is two times that produced by methanol in the direct methanol fuel cell. However, in order to achieve complete oxidation, C—C cleavage must occur without significant poisoning of the catalyst by C_1 intermediates. For that reason, breaking the C—C bond of ethanol and the selectivity of the electrocatalyst toward the formation of CO_2 as the final reaction product have been

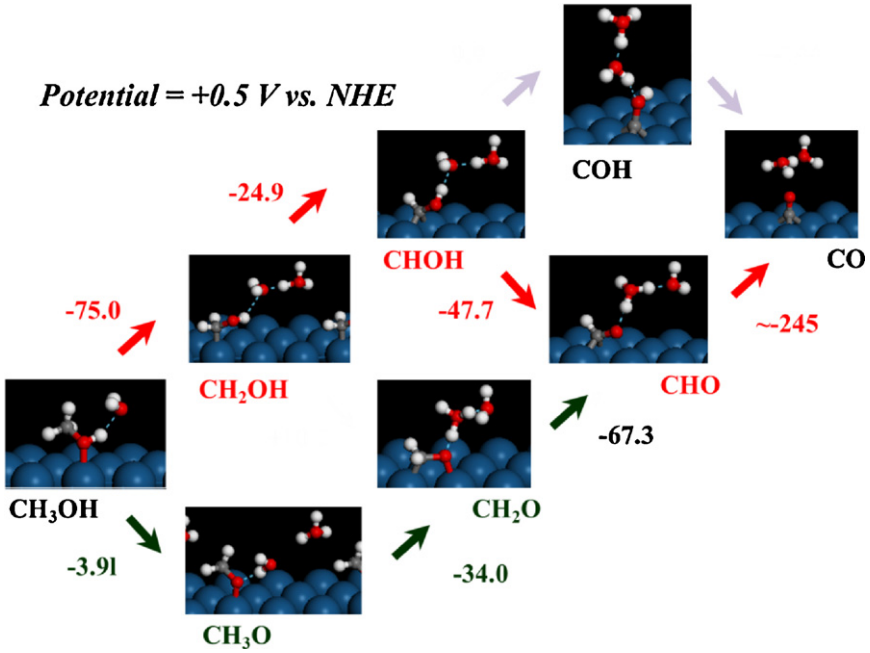

Fig. 3. DFT calculated potential-dependent reaction paths for the oxidation of methanol to CO over Pt(1 1 1). The onset potential for the dual path occurs at about 0.5 V. The primary path, available over a wide range potentials, is shown in red. It proceeds via a sequence of C—H bond activation steps ultimately forming the hydroxyl methylene intermediate (CHOH) before activating the final O—H bond to form CO. The minor path proceeds at 0.5–0.6 V RHE proceeds via the initial activation of O—H bond of methanol to form a surface methoxy intermediate which subsequently reacts to form formaldehyde consistent with previous speculations. The presence of steps that are likely present on the (1 1 1) surface reduces the onset potential to 0.4 V which is consistent with the experimental results [3,5].

identified as the major challenges for ethanol oxidation. The complete oxidation of ethanol to CO_2 is very difficult and only accounts for a few percent of the current that is generated.

Incomplete cleavage of C—C bonds results in partial oxidation pathways and the formation of acetaldehyde and acetic acid. These partial oxidation intermediates subsequently desorb from the surface and diffuse into the bulk electrolyte due to the concentration gradient of these species. As such, they are removed from the surface and do not undergo further oxidation thus resulting in a significant loss in efficiency since only a small fraction of the ethanol is fully oxidized. Evidence for these bulk related processes comes mostly from IR spectroscopy.

Our BB-SFG studies also provide a more in-depth treatment of the surface intermediate and show that within 3 min, a monolayer surface of CO has formed, indicating that it is apparently easy to break the C—C bond. Two other strongly bound surface intermediates, however, are formed which are absent in methanol oxidation: adsorbed acetate at higher potentials (demonstrating the difficulty of breaking the C—C bond) and $-CH_x$ species at lower potentials [31,32]. Consequently, these additional species tend to block surface sites and inhibit ethanol oxidation under acidic conditions. The electrocatalytic oxidation of ethanol over Pt electrodes in acid has two predominant limitations that prevent its viability [88]:

(1) The predominant partial oxidation leads to the formation of acetaldehyde and acetic acid thus resulting in the production of 2 or 4 electrons which are minor contributions to the current. Both acetate and acetic acid are also unwanted side products in the electrocatalytic oxidation.
(2) The path to C1 oxidation is rather complex as it requires breaking the C—C bond and removal of both $-CH_x$ and CO from the surface. Both of these tend to poison the surface at lower potentials.

7. Spectroscopic information on ethanol electrocatalysis by sum-frequency generation

Fig. 4a demonstrates that CO as one of reaction intermediates during ethanol oxidation accumulates on the Pt catalyst surface at low potentials and shows that the ethanol carbon–carbon bond

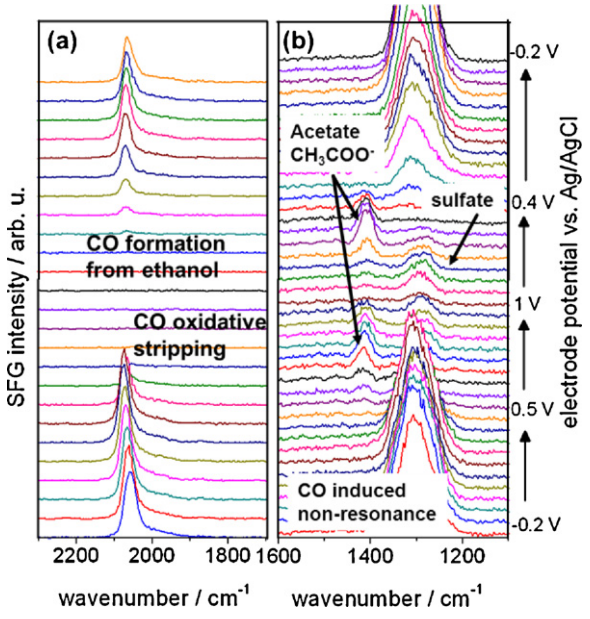

Fig. 4. Broadband SFG spectra in (a) the CO and (b) acetate spectral regions during the electrooxidation of 0.1 M ethanol on a polycrystalline Pt disk.

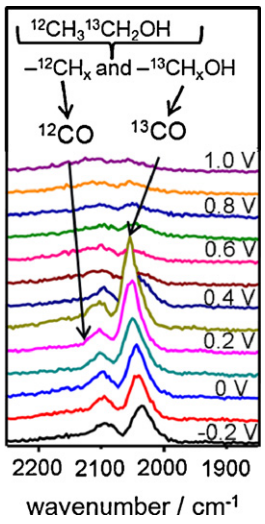

Fig. 5. Broadband SFG spectra in the CO spectral region that were recorded during the electrooxidation of 0.1 M $^{12}CH_3{}^{13}CH_2OH$ isotopically labeled ethanol on polycrystalline Pt.

can be broken under these conditions. The CO adlayer is oxidatively removed from the Pt surface as the electrode potential is increased above 0.4 V vs. Ag/AgCl thus resulting in a dramatic decrease in the intensity of the CO vibrational band. SFG spectra at $E > 0.6$ V in Fig. 4a appear featureless and indicate the absence of adsorbed CO for these potentials. In addition to a direct observation of CO vibrational bands, the non-resonant contribution $\chi^{(2)}_{NR}$ to the second-order susceptibility $\chi^{(2)}$ (see above) can be used to track changes in the CO adlayer. In Fig. 4b the non-resonant contribution arises at ~1300 cm^{-1} and is shaped by the Gaussian spectrum of the broadband IR pulse. A close inspection of Fig. 4b reveals that between 0.2 and 0.4 V $\chi^{(2)}_{NR}$ is strongly coupled to the presence of the CO adlayer and is consequently significantly decreased during the oxidation of CO [31,32,50]. After the CO adlayer has been stripped off of the Pt surface at potentials >0.4 V, Pt surface sites become available for other more weakly adsorbed molecular species such as acetate or (bi)sulfate (in sulfate media). In fact, vibrational bands at 1400 cm^{-1} and 1280 cm^{-1} are observed (Fig. 4b). These bands can be assigned to symmetric carboxylate ($-COO^-$) stretching vibrations of adsorbed acetate (1410 cm^{-1}) and S—O stretching vibrations of co-adsorbed (bi)sulfate anions (1280 cm^{-1}). The acetate band at 1410 cm^{-1} arises at $E > 0.6$ V, increases in intensity with increasing potential, reaches a local maximum and subsequently decreases to negligible intensities prior to 1.0 V. On the cathodic sweep, a similar intensity-potential profile is observed in the same potential region. Kutz et al. [31,32] compared the SFG amplitudes A_q of acetate and (bi)sulfate bands as a function of the applied potential in $HClO_4$ and H_2SO_4 electrolytes and showed that the co-adsorption of acetate and (bi)sulfate leads to a cooperative effect where the acetate adlayer can be observed in a wider potential range, where co-adsorbed (bi)sulfate confines the acetate anions on the Pt surface in a more ordered fashion [31,32].

Once the acetate is desorbed and surface oxides are removed, the CO vibrational band reappears on the cathodic sweep and a dense CO adlayer is formed again on the surface (Fig. 5). The acetate anion, however, does not oxidize within the potential range in which fuel cells operate and thus either diffuses from the surface as acetic acid (step (g) in Scheme 1, see below) or blocks Pt catalyst sites. The stabilization of acetate on the surface by (bi)sulfate co-adsorption additionally discourages the use of dilute sulfuric acid as an electrolytic medium for fuel cells, since the reaction pathway in which

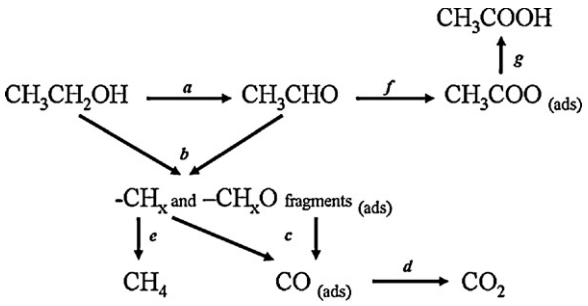

Scheme 1. Proposed reaction pathways for the electrooxidation of ethanol on a platinum surface in acidic electrolytes (Ref. [31] compared to that in Ref. [34]).

acetate and acetic acid are produced yields only four electrons per ethanol molecule and is therefore undesirable.

Further information on the oxidation of the different carbon species $-CH_3$ and $-CH_2OH$ of ethanol can be gained by the use of isotopically labeled $^{12}CH_3{}^{13}CH_2OH$ molecules since CO vibrational bands of both ^{12}CO and ^{13}CO are clearly resolved and are indicative of the oxidation of ethanol fragments according to step (c) in Scheme 1. The coverages of ^{13}CO and ^{12}CO are not identical, however, as we observe a greater quantity of ^{13}CO formed from the $-^{13}CH_xO$ fragment. Because the latter fragment is already partially oxidized, further oxidation to CO is far more facile than the oxidation of $-^{12}CH_x$ fragments [31,32]. Although a small fraction of the $-CH_x$ species can oxidize to CO at potentials as low as −0.2 V, the majority of the $-CH_x$ species possibly persists on the catalyst surface at higher potentials or is reduced to methane at cathodic potentials. A complete reaction scheme based on our experiments and additional evidence reported in the literature is proposed in the diagram (Scheme 1) for ethanol decomposition on platinum surfaces shown below. It should be pointed out, that acetyl which is a dehydrogenated product that results from acetaldehyde, was not included in Scheme 1 since at the present it has not been observed with BB-SFG. Note, that the BB-SFG method is only sensitive to the adlayer adjacent to the electrode surface the absence of strong acetyl related bands in our spectra suggests that there is no adsorbed acetyl in the first surface layer. Although, there could be the possibility that the acetyl species is SFG inactive and does not contribute to the SFG spectrum, it appears to be rather unlikely since similar adsorbates such as acetate is identified with SFG [31,32,50].

8. Theoretical efforts in ethanol electrocatalysis

In order to gain further insights into the possible elementary steps involved in the pathways for ethanol oxidation presented in Scheme 1, first principle DFT calculations were carried out over model Pt(1 1 1) and Pt(2 1 1) surfaces [89,90]. The calculations examine the first order effects of potential by shifting the reaction energies to reference them to the standard hydrogen electrode using the approach developed by Nørskov et al. [62]. The results do not include the solution phase or the potential dependent changes in the capacitance or charging of the surface.

Reaction energies were calculated for various plausible paths involving C—H, O—H and C—C bond activation steps. The specific paths examined and the resulting reaction energies are shown at 0 V over the Pt(1 1 1) and Pt(2 1 1) surfaces in Fig. 6a and c, respectively. On Pt(1 1 1) at 0 V, the results show that the initial activation of ethanol is much more likely to occur at the C—H rather than the O—H bond of the alcohol $-CH_2OH$ group. This is consistent with the previously reported theoretical and experimental results for methanol oxidation discussed above [55]. The subsequent activation of the O—H bond of the hydroxylethyl intermediate (RCH*OH) to form the observed acetaldehyde intermediate is thought to proceed as the next step in the sequence, although it is not the most thermodynamically favored route at lower potentials as it is endothermic by 1.07 eV. Increasing the electrode potential, however, shifts the energies for all of the electrochemical reaction steps which release an electron down by an energy which is directly proportional to the number of electrons released. The results presented in Fig. 6c indicate that as the potential is increased to 0.68 V RHE the two step path to acetaldehyde becomes favorable (exothermic). This is consistent with previous reported results for the activation of methanol over ideal Pt(1 1 1) surfaces [3].

As was discussed for methanol oxidation, it is well established that the ideal Pt(1 1 1) surfaces, contain step defect sites that can be considerably more reactive. This is consistent with results that show that increases in surface step density increase the current [91]. The Pt(2 1 1) surface was, therefore, used as a simple model of step sites. The results for the activation of ethanol on the Pt(2 1 1) surfaces which are shown in Fig. 6c, indicate that the two paths for the activation of ethanol have very similar reaction energies. The activation of O—H is decreased by over 0.9 eV at the step edges over that on the Pt(1 1 1) surface as is shown in comparing the results in Fig. 6a with those in Fig. 6c. The results in Fig. 6d indicate that the route of ethanol to acetaldehyde now becomes exothermic (on Pt(2 1 1)) at an onset potential of 0.38 V RHE which is consistent with the experimental results that show onset potentials close to 0.4 V RHE. This suggests that the current at these low-potential may be the result of steps or defect sites as was previously suggested [91,92].

In order to achieve complete oxidation of ethanol to CO_2, the C—C bond must be activated. The results shown in Fig. 6a for the activation of ethanol over Pt(1 1 1) surface indicate that C—C bond breaking reactions become increasingly more exothermic as we increase the degree of dehydrogenation of ethanol. We confirmed this in recent studies that examined the activation barriers for a number of C—C cleavage reactions of the acetaldehyde intermediate and further dehydrogenated intermediates as is shown in Fig. 7 [92,93]. The activation barrier for C—C cleavage of acetaldehyde was found to be 1.55 eV, compared to 0.92 eV for the dehydrogenated CH=C=O ketene-like intermediate. As was observed for O—H activation, C—C activation is also more facile over step-like defect sites modeled by a (2 1 1) surface as shown in Fig. 6c. On Pt(2 1 1), all but one of the C—C activation steps were calculated to be exothermic. As the potential is increased, the dehydrogenation reactions become linearly more exothermic, whereas the C—C activation steps remain unaffected as they are not explicitly potential dependent. This indicates that as the potential is increased, C—C cleavage is more likely to occur via one of the more-dehydrogenated surface intermediate. For example, Fig. 6c shows that at 0 V, C—C activation of the CH_3CHOH is exothermic by −0.52 eV, whereas that to activate the C—C bond of acetaldehyde is endothermic by +0.14 eV. At 0.38 V RHE, the dehydrogenation barrier to form acetaldehyde becomes exothermic with a reaction energy of −0.24 eV as is shown in Fig. 6d. This is consistent with experimental results which suggest that at potentials ≤0.4 V RHE, C_1 intermediates are formed via C—C cleavage of ethanol or a partially dehydrogenated intermediate such as CH_3CHOH. Whereas for potentials > 0.4 V RHE, the C—C cleavage step is thought to occur through activation of acetaldehyde [92,88].

At all potentials <0.7 V RHE, it appears that the current is limited by the unavailability of metal sites on the ideal Pt(1 1 1) surface that can activate the O—H and C—C bonds. As discussed, these reactions are much more facile over steps and defect sites that are present even on the ideal Pt(1 1 1) surfaces used experimentally. While the defect sites clearly enhance the activation of the initial activation of the C—O and C—C bonds, they are likely to be poisoned by strongly bound C_1 intermediates form especially at lower potentials. For that reason, as previously mentioned, many efforts have been made

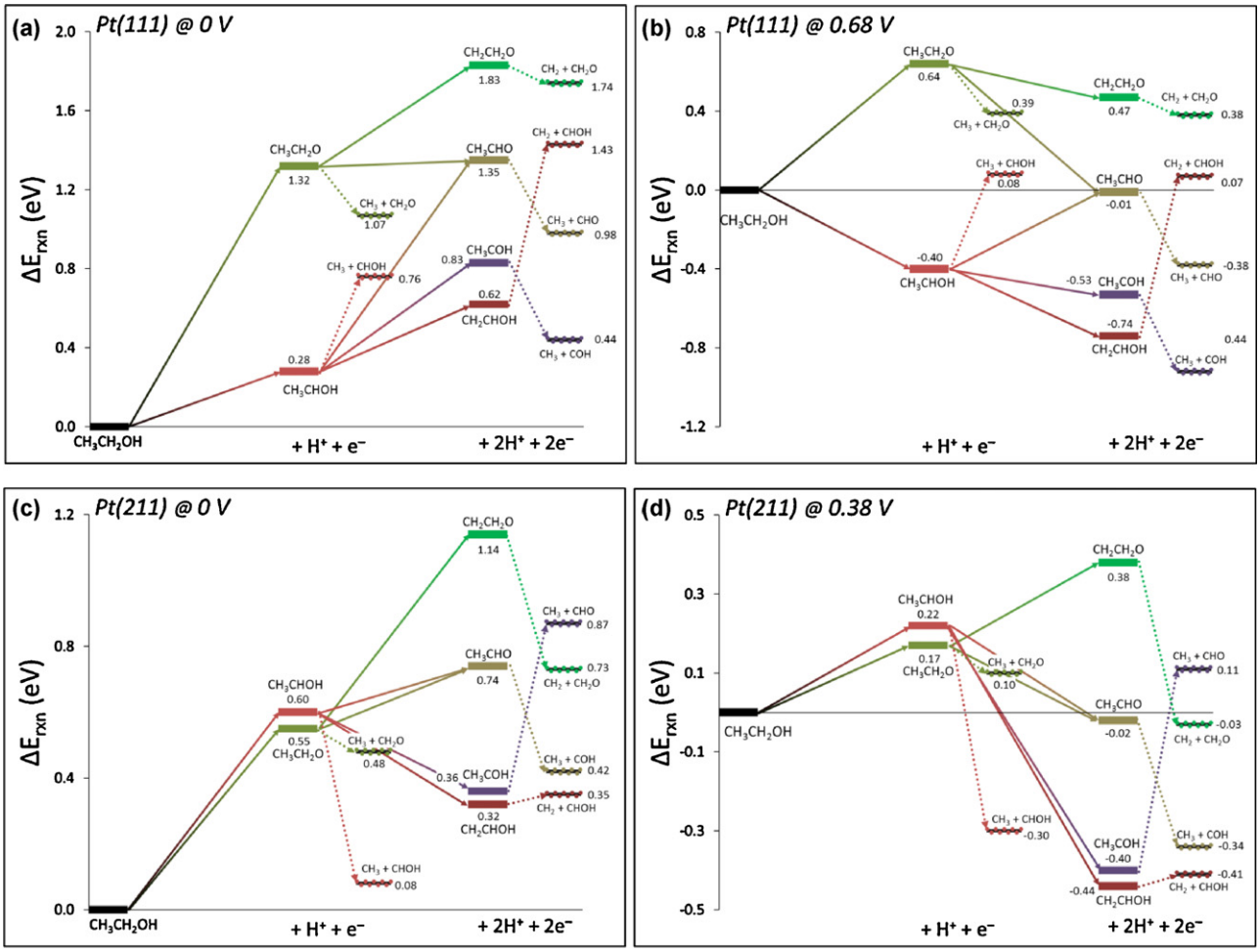

Fig. 6. Reaction energies of elementary steps (referenced to adsorbed ethanol) for dehydrogenation and C—C cleavage reactions (dashed lines) for (a) Pt(1 1 1) at 0 V and (b) 0.68 V RHE and for (c) Pt(2 1 1) at 0 V and (d) 0.38 V RHE.

to alloy Pt with other more oxophilic metals such as Ru and Sn which help to facilitate the oxidation of the C_1 intermediates. It is thought, that the main role of Ru and Sn in these alloys is to activate water, generating surface-bound hydroxyl intermediate (OH*), which assists in C_1 oxidation [94–98].

On pure Pt, the activation of water to form surface hydroxyl intermediates occurs at potentials > 0.63 V. DFT calculated phase diagrams of the water/Pt(1 1 1) interface indicate that water is the most stable surface intermediate between 0.08 and 0.63 V [99]. Water, however, activates at 0.63 V and form stable hydroxyl (OH*) intermediates on the surface. The presence of defect sites, however, significantly lowers the potentials for the activation of water. The formation of these surface OH* and O* intermediates can significant influence and alter the surface chemistry as both species tend to lower the activation barriers for proton transfer and thus facilitate hydrogen abstraction reactions.

The oxidation of acetaldehyde to acetic acid and acetate intermediates also likely occur through reaction with surface-bound

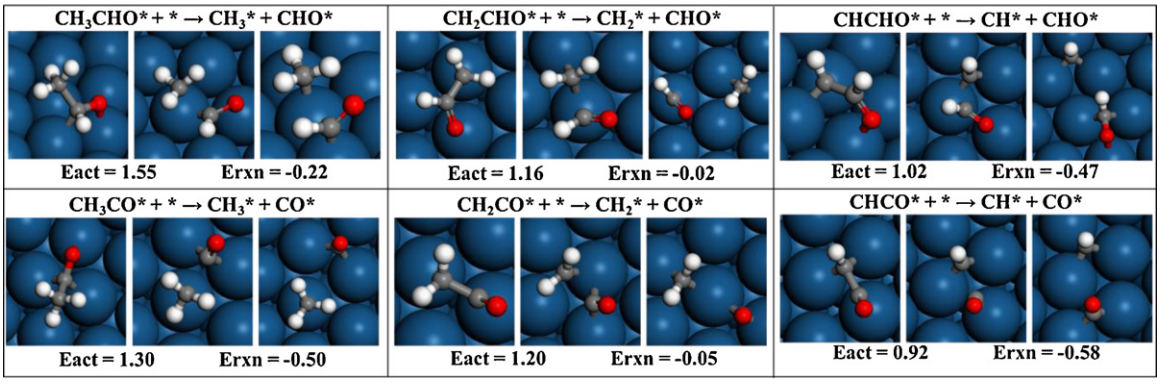

Fig. 7. Various C—C cleavage reactions of dehydrogenated acetaldehyde intermediates on a Pt(1 1 1) surface at 0 V [92,88].

OH* intermediates. The addition of OH* to the aldehyde results in the formation of a substituted CH_3CHOH-O* alkoxide intermediate on the electrode which subsequently dehydrogenates to give acetic acid as well as acetate. This is consistent with experimental results, which shows that the oxidation of acetaldehyde takes place near 0.7 V, forming mostly acetic acid [100]. Furthermore, OH* can facilitate removal of strongly bound CO* species through: $OH^* + CO^* \rightarrow CO_2 + H^+ + e^-$

Thus, it appears that the shift at potentials of 0.6 V RHE from CO-covered to acetate-covered surface seen in the BB-SFG results is due to ability to activate water at those higher potentials to form the surface OH* species. Once OH* is present are formed, they can readily oxidize the CO species to form CO_2, and react with acetaldehyde to form the observed acetate species and acid products. These OH*-driven mechanisms are also observed in alkaline anion exchange fuel cells (AAEFCs) and in aerobic oxidation in heterogeneous catalysis operating in aqueous phase at high pH as will be discussed in further detail in the next section.

9. Synergy between electrocatalysis and heterogeneous catalysis

Many of the fundamental constructs in electrocatalysis have direct analogies with heterogeneous catalysis as both are often carried out over supported metals where the metal is critical in the adsorption of the reactants, the activation of surface intermediates, stabilizing transition states and reaction intermediates and controlling the molecular transformations. In addition, the metal/support interaction present in both catalysis and electrocatalysis is important as it controls catalyst stability, particle size, electronic effects, spillover phenomena, as well as the formation of bifunctional sites. While there is significant degree of overlap and synergies between catalysis and electrocatalysis, there are also unique differences between the two that often result from the presence of electrified metal/solution interfaces that occurs in electrocatalysis. We restrict our discussions here to the comparison of catalysis and electrocatalysis over metal particles.

Heterogeneous catalysis often takes place in gas phase over metal surfaces which allow one to take advantage of the significant advances in in situ spectroscopic measurements, isotopic labeling and comprehensive kinetic studies to establish detailed insights into reaction mechanism. A significant database of fundamental knowledge has been established for catalytic reactions that occur on metal surfaces which has, and will continue to, assist in understanding of catalysis as well as electrocatalysis. Many of the most active metals used in electrocatalysis are very often the same as those used in heterogeneous catalysis. For example, Pt and other group VIII metals are known to be very active for fuel cells, automotive exhaust, hydrogenolysis, and hydrogenation catalysis. Group VIII metals are often present in heterogeneous catalysis and electrocatalysis as a result of the well-established Sabatier's principle which suggests that the metals in middle of the periodic table demonstrate optimal metal-adsorbate bond strengths necessary to drive surface reactivity and still allow product desorption [101–105].

The complex aqueous phase and the buried interfaces that are present in electrocatalysis have made it much more challenging to provide molecular level insights into how these reactions proceed. As a result electrocatalysis has often followed from the advances in heterogeneous catalysis. The exponential rise in fundamental research efforts in the catalytic conversion of biomass derived intermediates over supported metal catalysts in solution, however, have begun to reverse this trend. Many of the issues involving the metal/support stability and reaction mechanisms that now arise in aqueous phase heterogeneous catalysis are essentially the same as those that have already been solved in electrocatalysis. We are beginning to recognize a growing important trend where there is a significant transfer of knowledge from electrocatalysis back to heterogeneous catalysis. We present herein just a few areas concerning reaction mechanisms for both aqueous phase heterogeneous catalysis as well as electrocatalysis in order to highlight the similarities and differences between the two. A fundamental understanding of the similarities and difference should help to advance both areas.

The oxidation of alcohols is one area in which there is significant synergy between electrocatalysis and heterogeneous catalysis. As was discussed previously in the manuscript, the electrocatalytic oxidations of methanol and ethanol have been extensively examined in acidic PEMFCs as well as in alkaline anion exchange fuel cells (AAEFCs). Similarly, a number of researchers have now shown that polyols, such as glycerol and glucose, can be oxidized in fuel cells [103–105,121]. The area is important for both catalysis and electrocatalysis as we witnessed an exponential rise in the number of papers on the catalytic oxidation of alcohols and polyols over supported metals as result of their important in the conversion of biorenewable intermediates to chemicals.

Recent reports on the selective oxidation of alcohols such as ethanol, glycerol, glucose and hydroxymethylfurfural to mono- and di-acids over aqueous-phase heterogeneous catalysts indicate that the presence of alkaline media strongly promotes the activity and selectivity toward acid products over Pt and Pd catalysts across a range of alcohol substrates. Furthermore, the oxidation of ethanol and glycerol were found to be over an order of magnitude more active over supported Au catalysts. As shown in Table 1 glycerol is selectively oxidized over Au/C at pH near 12 to glyceric acid with greater than 60% selectivity with glycolic acid being the main byproduct [106]. Isotopic labeling was used to show that the source of additional oxygen in the acid products results solely from the OH/H_2O system, rather than the O_2 co-reactant. While no activity was observed for alcohol oxidation over Au/C in the absence of base, both Pt/C and Pd/C show lower activities with limited selectivity to acid products, instead generating glyceraldehyde and dihydroxyacetone, which are the products of oxidative dehydrogenation. On Pt/C, a series of experiments were run varying the NaOH:glycerol

Table 1
Aqueous-phase heterogeneous glycerol oxidation over Au/C and Pt/C published in Zope et al. [106].

Catalyst	NaOH:glycerol (mol:mol)	TOF (s^{-1})	Conversion (%)	Selectivity (%)				
				Glyceric acid	Glycolic acid	Tartronic acid	Glyceraldehyde	Dihydroxy-acetone
Au/C[a]	2.0	6.1	6.8	67	33	0.0	0.0	0.0
Au/C[b]	0.0	0.0	0.0	0.0	0.0	0.0	0.0	0.0
Pt/C[a]	2.0	1.6	16	70	21	7.0	0.0	0.0
Pt/C[a]	1.0	0.76	7.1	78	14	7.0	0.0	0.0
Pt/C[a]	0.5	0.48	4.7	72	28	0.0	0.0	0.0
Pt/C[b]	0.0	0.06	9.0	25	0.0	0.0	54	21

[a] Reaction conditions: 0.3 M glycerol (G), 0.6 M NaOH, 30 mL, 333 K, pO_2 150 psig, G:Au = G:Pt = 8000 (mol:mol), G:Pd = 2500 (mol:mol), t = 0.5 h.
[b] Reaction conditions: 0.3 M glycerol (G), 5 mL, 333 K, pO_2 150 psig, G:Au = G:Pt = 5000 (mol:mol), G:Pd = 2000 (mol:mol), t = 5 h; gold particle sizes: Au/C = 10.5 nm, Au/TiO_2 = 3.5 nm; dispersion: Au/C = 0.05, Au/TiO_2 = 0.29, Pt/C = 0.43, Pd/C = 0.33 (31).

Table 2
Selected DFT results on the oxidation of ethanol and the oxygen reduction reaction in aqueous solvent, from Zope et al. [106]. All of the reported energies are given in units of kJ/mol.

Reaction	Au (1 1 1)	
	w/solvent	
	ΔH_{RXN}	E_{ACT}
$CH_3CH_2OH^* + * \rightarrow CH_3CH_2O^* + H^*$	196	204
$CH_3CH_2OH^* + OH^* \rightarrow CH_3CH_2O^* + H_2O^*$	13	22
$CH_3CH_2O^* + * \rightarrow CH_3CHO^* + H^*$	−40	46
$CH_3CH_2O^* + OH^* \rightarrow CH_3CHO^* + H_2O^*$	−222	12
$CH_3CHO^* + OH^* \rightarrow CH_3CH(OH)O^* + *$	−33	5
$CH_3CH(OH)O^* + * \rightarrow CH_3COOH^* + H^*$	−151	21
$CH_3CH(OH)O^* + OH^* \rightarrow CH_3COOH^* + H_2O^*$	−334	29
[a] $CO^* + OH^* \rightarrow CO_2 + H^+ + e^-$	−230	0
$OH^* + H^* \rightarrow H_2O^* + *$	−183	39
$O_2^* + * \rightarrow O^* + O^*$	41	105
$O_2^* + H^* \rightarrow OOH^* + *$	−161	25
$O_2^* + H_2O^* \rightarrow OOH^* + OH^*$	−4	16
$OOH^* + * \rightarrow OH^* + O^*$	−56	83
$OOH^* + H^* \rightarrow HOOH^* + *$	−146	19
$OOH^* + H_2O^* \rightarrow HOOH^* + *$	37	48
$HOOH^* + * \rightarrow OH^* + OH^*$	−86	71

[a] From this work.

ratio. The observed TOF was shown to be linearly proportional to the concentration of base, indicating that the rate-limiting-step of the reaction is first order in hydroxide concentration. This is consistent with studies of electro-oxidation of ethanol over Au electrodes which show a near-logarithmic relationship between activity and pH [88]. These results demonstrate that glyceraldehyde and dihydroxyacetone are likely the primary products of oxidation, followed rapidly (for systems at high pH) by further oxidation to form glyceric acid.

The role of the catalyst during this further oxidation is unclear. Zope et al. [106] suggest that the catalyst is necessary for carrying out the subsequent C—H bond activation of the gem-diol intermediate that forms. Electrocatalytic experiments carried out by Lai et al., however, suggest that the subsequent reactions are carried out instead solely by the base in solution. Glyceraldehyde is not stable in solution at high pH [107], and that with O_2 present [108], the aldehyde can decompose into a number of products. Under electrochemical conditions the decomposition produced equimolar amounts of glycolic and formic acids. These products, however, were not seen in this study over supported heterogeneous catalysts [107]. Furthermore, if the catalyst's role is only to facilitate β-H elimination in forming the aldehyde intermediates, then it would be unlikely to observe different selectivities of secondary products on different metals, as is shown in Table 2 where the selectivity to C_2 acids is slightly higher for Au/C than for Pt/C. Although the cause of these shifts is unknown, it has been shown [107] that H_2O_2, an observed byproduct of the oxygen reduction reaction, leads to greater amounts of C—C cleavage.

Recent studies on electrooxidation of glycerol over Pt and Au electrodes show direct similarities with this work but also reveal interesting differences [109]. Au electrodes are significantly more active, albeit at higher potentials, than their Pt counterparts and demonstrate higher selectivity toward C—C cleavage reactions. Although, in the case of Au electrodes, the presence of formic acid was detected and the selectivity toward C—C cleavage products was much higher than the selectivity to glyceric acid, which contrasts the results found over heterogeneous gold catalysts. As previously mentioned, glyceraldehyde decomposition has been shown to form equimolar amounts of glycolic and formic acids [108,110]. This solution-phase degradation is likely to be the dominant pathway over Au electrodes; however, on Pt where the aldehyde is more likely to remain chemisorbed to the surface, oxidation via surface hydroxide is the more likely path. This competition between desorption (leading to degradation) and further oxidation on the surface could explain the dramatic differences in glyceric acid selectivity observed between the Au and Pt electrodes.

DFT calculations were carried out which explore the roles of hydroxide and the metal during the oxidation of ethanol. These calculations demonstrated that OH species on the Au surface promote the activation of both the O—H and C—H bonds in the dehydrogenation of alcohol to the aldehyde via the reactions shown in Eqs. (1) and (2). The aldehyde intermediate that results can easily desorb and hydrate in the solution phase through a base-catalyzed mechanism, thus yielding a geminal diol intermediate (Eq. (3)). Once formed, the geminal diol intermediate can readily deprotonate in solution or on the surface yielding a stable surface alkoxide intermediate. (Eq. (4)) The C—H bond of the alkoxide is subsequently activated by surface-bound hydroxide or directly over the metal thus resulting in formation of acetic acid (Eq. (4)). The energetics for these reactions are given in Table 2.

$$CH_3CH_2OH + OH^- \rightarrow CH_3CH_2O^- + H_2O \rightarrow CH_3CH_2O* + e^- \quad (1)$$

$$CH_3CH_2O* + OH* \rightarrow CH_3CH{=}O* + H_2O* \quad (2)$$

$$CH_3CH{=}O + OH^- + H_2O \rightarrow CH_3CHOOH^- + H_2O \rightarrow CH_3CH(OH)_2 + 2H_2O \quad (3)$$

$$CH_3CH(OH)_2 + 2OH* \rightarrow CH_3CHOOH^* + H_2O + OH* \rightarrow CH_3COOH + 2H_2O \quad (4)$$

$$OH^- \leftrightarrow OH^* + e^- \quad (5)$$

The ability of hydroxide to act as a nucleophile during the oxidation/hydration of the aldehyde intermediates is very similar to the widely examined electrocatalytic oxidation CO. As discussed previously, CO species are commonly observed at high coverage during alcohol oxidation over Pt and other group VIII metals as was presented above in the BB-SFG results over Pt. However, heterogeneous CO oxidation has also demonstrated high activity on Au/C catalysts [111]. In both cases, it is believed that the CO-removal mechanism often occurs through reaction with hydroxide-bound species.

$$CO* + OH* \rightarrow COOH* \rightarrow CO_2(aq) + H^+ + e^- \quad (6)$$

DFT calculations were carried out over model Au(1 1 1) surfaces in the presence of discrete water molecules to examine in more detail the mechanism of this reaction and charge transfer over bulk Au in alkaline media. The results, which are summarized in Fig. 8, demonstrate that the two-step reaction is essentially barrier-free and highly exothermic. In order to localize atomic charges and follow the evolution of charge as a function of the reaction coordinate, the wavefunctions of the DFT calculations were restructured into a series of quasi-atomic-minimal basis set orbitals (QUAMBO) [112], which enabled a Mulliken charge analysis. The results from the charge analysis depicted in Fig. 8 show that as CO* and OH* combine on the surface and release 0.4 electrons that directly transferred to the metal. Once the COOH* intermediate is formed, it rapidly deprotonates into solution, followed by CO_2 desorption, which transfers another 0.4 electrons into the metal surface. Through the deprotonation of COOH*, the water phase also loses 0.3 electrons over the course of the reaction; a total of 1.1 electrons are deposited into the metal surface. This demonstrates the decoupling of the proton and electron shown in Eq. (6).

At neutral or slightly acidic pH, Au is inactive for both selective heterogeneous oxidation as well as electrooxidation [91,106,107].

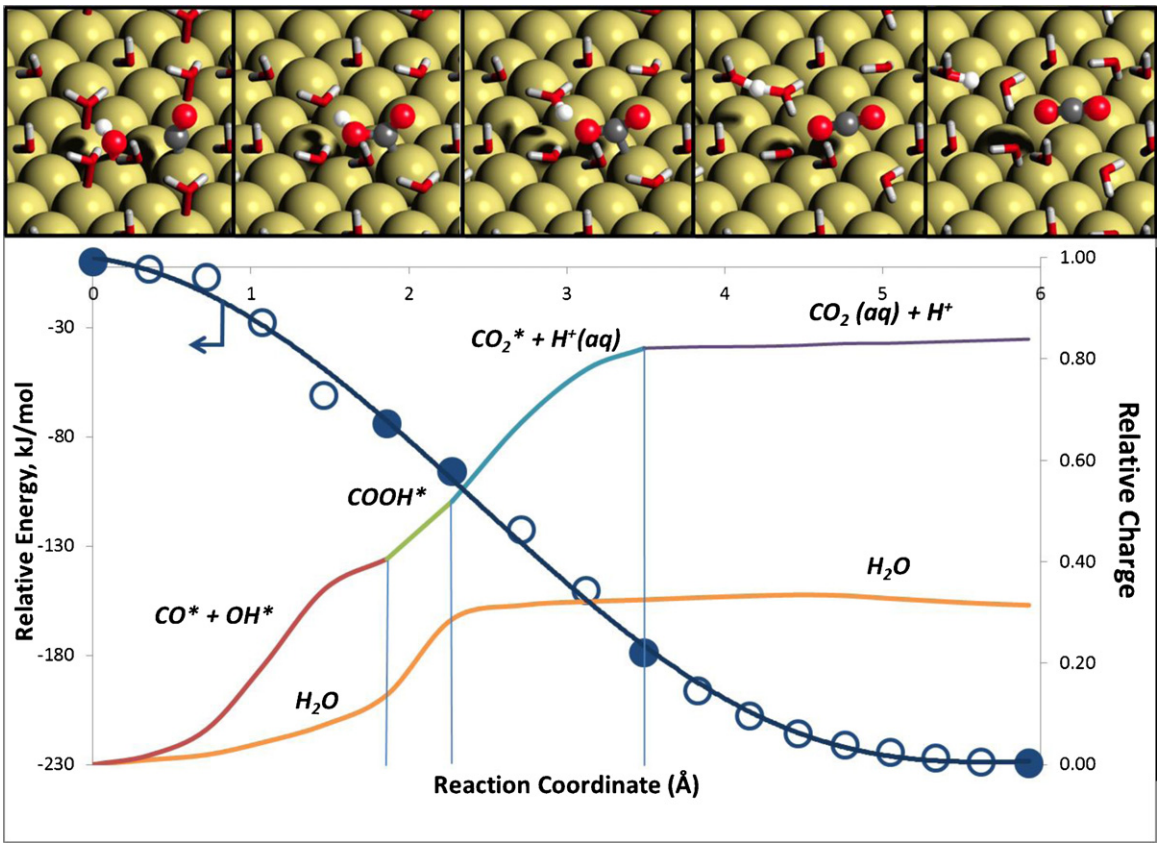

Fig. 8. Calculated minimum energy pathway for CO oxidation to CO_2 on a Au catalyst with surface hydroxide species. Filled circles correspond to the images along the minimum energy reaction path shown above the plot. Also shown is the change in charge on the reactants and solvent. The change in charge on the metal is the same as the change in charge on the reactants and solvent (but opposite in magnitude).

While the rates for the heterogeneous and low-potential electrocatalytic oxidation of alcohols over Pd and Pt are very low at neutral and acidic conditions, they increase significantly in the electrocatalytic systems with increases in the potential as was previously discussed. During selective heterogeneous oxidation, it is unclear whether there is a change in mechanism due to the reduced availability of hydroxide. Recent theoretical studies on the selective oxidation of ethanol oxidation over Pd(1 1 1) [113] conclude that the reaction proceeds via C—H activation of the alcohol to form the RC*HOH hydroxyalkyl intermediate over the metal rather than by O—H activation via surface or solution phase OH intermediates. This is consistent with the known electrocatalytic pathways for the oxidation of methanol and ethanol carried out in acidic media as was discussed earlier. The subsequent activation of the C—H or O—H bond of the adsorbed hydroxyalkyl intermediate to form the RC-OH intermediate or the aldehyde, respectively, were found to have similar activation barriers. As that work was focused on selective oxidation to form organic acids, it did not examine the nature of the C—C bond activation. The work does, however, reveal similarities between ethanol electrooxidation in acid media and neutral-pH selective heterogeneous oxidation.

$$CH_3CH_2OH* + * \rightarrow CH_3CHOH* + H* \quad (7)$$

$$CH_3CHOH* + * \rightarrow CH_3COH* + H* \text{ or } CH_3CHO* + H* \quad (8)$$

The heterogeneous catalytic oxidation mechanism thus does not require the direct reaction or interaction with the O_2 co-reactant which is similar to electrocatalytic systems where the alcohol and O_2 co-reagents react in isolated half-cells. The role of O_2 in the catalytic system is to consume electrons produced during the oxidation reaction via the oxygen reduction reaction which is essentially identical to that found in electrocatalysis. In the heterogeneous catalytic system, these two processes take place in concert, creating a single-particle electrochemical cell, where the metal nanoparticle acts as an electron reservoir. In electrocatalysis, the oxidation and reduction reactions occur at separate electrodes.

The ORR mechanism has been the subject of numerous electrochemical studies [114–120], as research into reducing the amount and cost of the catalyst at the cathode has been a major focus in current fuel cell research. In heterogeneous catalysis, ORR mechanisms that are thought to be operative in the selective heterogeneous oxidation over Au and Pt have been examined by density functional theoretical calculations [106,113]. DFT results indicate that under the conditions used for alcohol oxidation, oxygen reduction occurs via the reaction between oxygen and water to generate peroxide species on the surface. These peroxide species can readily dissociate over Pt and Pd, thus resulting in the formation of O* and OH* intermediates. Au, however, cannot readily activate the O—OH bond and is thus further reduced to form hydrogen peroxide, an observed reaction byproduct, some of which is likely to dissociate, reforming hydroxide consumed during the reaction. Further reduction of hydroxide to water is also likely, consuming any atomic hydrogen generated on the surface. This is similar to work in electrocatalysis, which has indicates that under acidic conditions, O_2 does not initially dissociate, but instead is reduced via reaction with a proton in solution (and an electron of the electrode) to form OOH* species which then dissociates [120,121]. Peroxide species have also been observed and lead to undesired side-reactions and catalyst instability [120].

$$O_2* + 2H_2O* \rightarrow OOH* + H_2O* + OH* \rightarrow O* + H_2O + 2OH* \rightarrow 4OH* \quad \text{Pd/Pt:} \quad (9)$$

$$O_2* + 2H_2O* \rightarrow OOH* + H_2O* + OH* \rightarrow HOOH* + 2OH* \rightarrow 4OH* \quad Au: \tag{10}$$

$$OH* + H* \rightarrow H_2O* \tag{11}$$

It is clear that there are some obvious similarities between heterogeneous and electrocatalysis. In the selective oxidation of alcohols, the heterogeneous catalytic system establishes a local electrochemical cell that directly mimics the oxidation and reduction behavior that occur at the anode and cathode of the PEM and AAEFC fuel cells. In addition, to the similarities, there are unique differences that often arise between heterogeneous catalysis and electrocatalysis. A more detailed understanding of the similarities and differences will clearly help to advance both the fields of catalysis and electrocatalysis.

10. Conclusions

Electrocatalysis is perhaps the most challenging branch in all of catalysis as the chemistry is controlled by the complex three phase interface that results between the metal, aqueous media/polymer electrolyte and carbon support as well as by the applied potential. This interface dictates the catalyst stability, morphology and reaction mechanism, and interestingly mimics may of the features found in aqueous-phase heterogeneous catalytic systems. The advances that have occurred over the past decade in in situ as well as ex situ spectroscopy, characterization, and first principle simulations begin to allow for the much more in-depth interrogation and understanding of catalysis at such complex interfaces. The detailed understanding of the similarities and differences between the electrocatalytic as well as aqueous phase catalytic systems should ultimately enable significant advances in both fields.

Studies in heterogeneous catalysis as well as electrocatalysis have shown that supported Pt and other group VIII metals as well as Au can carry out the oxidation of methanol, ethanol and other polyols but their activities and extents of oxidation are very strongly influenced by the reaction conditions and the reaction medium in which they carried out. These studies have shown that Au electrocatalysts are severely limited in neutral or acidic media, whereas Pt takes on limited reactivity at these same conditions, where its activity is proportional to hydroxide concentration. In situ BB-SFG spectroscopy show, that CO as well as other C_1 surface species that form as a result of the dehydrogenation of the alcohol dominate the surface at low pH/potential and limit catalytic reactivity. At higher potentials, CO^* is oxidized to off of the surface as CO_2, thus allowing other oxidized intermediates such as acetate and acetic acid to bind in their place.

These in situ spectroscopic studies together with first-principle DFT calculations offer a reliable picture of the understanding of activity and mechanism for methanol as well as ethanol oxidation. The results show that at low potentials/low pH, Pt is initially active, with defect sites likely responsible for the O—H and C—C bond cleavage. These sites, however, become poisoned with time by strongly bound C_1 intermediates, thus limiting the rates of oxidation of these species from the surface. At higher potentials, water is activated to form hydroxide intermediates that can readily oxidize the C_1 species from the surface. The surface hydroxyl intermediates can also activate the alcohol to form the corresponding aldehyde and in addition react with the aldehyde to form stable acid products which go on to form acetate intermediates that cover the surface. Furthermore, the acid products appear to be quite stable, preventing C—C activation and complete oxidation of ethanol to CO_2, which is the desired reaction.

The significant advances in spectroscopy, characterization, synthesis, theory and simulation as well as their synergistic integration have allowed enabled the community to begin to provide unique insights into the similarities and differences between catalysis and electrocatalysis. These insights provide for a stronger foundation of the fundamental chemistry and mechanistic features that control both catalysis and electrocatalysis and enable advances and developments across both fields. However, it is important to note that the advances discussed herein focus on model systems of these complex catalytic environments, whether in the form of idealized surface calculations or single-crystal surface science studies. Real fuel cell materials, such as supported metal nanoparticles, have many features which are not captured by these idealized models. These include the effects of particle size and under-coordinated sites on metal nanoparticles, the effects of the catalyst support, and ion and mass transport limitations, just to name a few. For these reasons it is important to understand the discrepancies between these model systems and real fuel cells as we continue to develop an understanding of the unique mechanistic chemistry.

Acknowledgments

AW would like to kindly acknowledge the support by the US Army Research Office under award W911NF-08-10309 and the National Science Foundation (under CHE 06-51083). BB gratefully acknowledges support by the Alexander von Humboldt Foundation and a Feodor Lynen fellowship. MN and DH would like to acknowledge Craig Plaisance for the implementation of QUAMBO methods into the VASP code. MN gratefully acknowledges support from the Office of Basic Energy Sciences under Award Number ERKCC61 for the work on metal/solution interfaces. (This work is part of the Fluid Interface Reactions, Structures and Transport (FIRST) Center, an Energy Frontier Research Center funded by the U.S. Department of Energy, Office of Science, Office of Basic Energy Sciences),U.S. Department of Energy, Division of Chemical Sciences, Office of Basic Energy Sciences (DE-FG02-07ER15894) for work on oxygen reduction and the National Science Foundation Research Center for Biorenewable Chemicals (EEC-0813570) and the National Science Foundation PIRE (NSF OISE-0730277) for the work on alcohol oxidation.

References

[1] G.A. Somorjai, I. Li, Introduction to Surface Chemistry and Catalysis, 2nd ed., Wiley, Hoboken, NJ, 2010.
[2] A.J. Bard, L.R. Faulkner, Electrochemical Methods, 2nd ed., Wiley, New York, 2001.
[3] D. Cao, et al., Mechanisms of methanol decomposition on platinum: a combined experimental ab initio approach, Journal of Physical Chemistry B 109 (23) (2005) 11622–11633.
[4] B. Hammer, J.K. Norskov, Theoretical surface science and catalysis – calculations and concepts, Advances in Catalysis 45 (2000) 71–128.
[5] T. Iwasita, Electrocatalysis of methanol oxidation, Electrochimica Acta 47 (22–23) (2002) 3663–3674.
[6] M.T.M. Koper, S.C.S. Lai, Ethanol electro-oxidation on platinum in alkaline media, Physical Chemistry Chemical Physics 11 (2009) 10446–10456.
[7] M. Neurock, A. Wieckowski, Contrast and synergy between electrocatalysis and heterogeneous catalysis, Advances in Physical Chemistry, in press.
[8] A. Wieckowski, J.K. Norskov, Fuel cell science: theory, fundamentals, and biocatalysis, in: A. Wieckowski (Ed.), Electrocatalysis and Electrochemistry, vol. 1, John Wiley & Sons, Hoboken, NJ, 2010, pp. 1–618.
[9] J.M. Petroski, et al., Kinetically controlled growth and shape formation mechanism of platinum nanoparticles, Journal of Physical Chemistry B 102 (1998) 3316–3320.
[10] J.B. Wu, et al., Truncated octahedral Pt(3)Ni oxygen reduction reaction electrocatalysts, Journal of the American Chemical Society 132 (14) (2010) 4984–4985.
[11] Z.Y. Zhou, et al., High-index faceted platinum nanocrystals supported on carbon black as highly efficient catalysts for ethanol electrooxidation, Angewandte Chemie-International Edition 49 (2) (2010) 411–414.
[12] S. Iijima, Science and industrial applications of nanocarbon materials such as fullerence, carbon nanotubes and graphenes, in: The 2011 WPI-AIMR Annual Workshop, Tohoku University, Sendai International Center, 2011.

[13] N. Tian, et al., Direct electrodeposition of tetrahexahedral pd nanocrystals with high-index facets and high catalytic activity for ethanol electrooxidation, Journal of the American Chemical Society 132 (22) (2010) 7580–7581.
[14] B.A. Rosen, et al., Ionic liquid-mediated selective conversion of CO(2) to CO at low overpotentials, Science 334 (6056) (2011) 643–644.
[15] B.E. Conway, W.G. Pell, Double-layer and pseudocapacitance types of electrochemical capacitors and their applications to the development of hybrid devices, Journal of Solid State Electrochemistry 7 (9) (2003) 637–644.
[16] W.G. Pell, B.E. Conway, Peculiarities and requirements of asymmetric capacitor devices based on combination of capacitor and battery-type electrodes, Journal of Power Sources 136 (2) (2004) 334–345.
[17] C. Joachim, J.K. Gimzewski, A. Aviram, Electronics using hybrid-molecular and mono-molecular devices, Nature 408 (2000) 541–548.
[18] M.A. Reed, et al., Conductance of a molecular junction, Science 278 (5336) (1997) 252–254.
[19] A.H. Fanney, et al., Comparison of photovoltaic module performance measurements, Journal of Solar Energy Engineering-Transactions of the ASME 128 (2) (2006) 152–159.
[20] D. Gust, T.A. Moore, A.L. Moore, Solar fuels via artificial photosynthesis, Accounts of Chemical Research 42 (12) (2009) 1890–1898.
[21] S.P. Ong, et al., Voltage, stability and diffusion barrier differences between sodium-ion and lithium-ion intercalation materials, Energy & Environmental Science 4 (9) (2011) 3680–3688.
[22] B.R. Long, et al., Dopant modulated Li insertion in Si for battery anodes: theory and experiment, Journal of Physical Chemistry C 115 (38) (2011) 18916–18921.
[23] S. Litster, G. McLean, PEM fuel cell electrodes, Journal of Power Sources 130 (2004) 61–76.
[24] M.N. Markovic, P.N. Ross, Surface science studies of model fuel cell electrocatalysts, Surface Science Reports 45 (2002) 117–229.
[25] S. Chen, et al., Platinum-alloy cathode catalyst degradation in proton exchange membrane fuel cells: nanometer-scale compositional and morphological changes, Journal of the Electrochemical Society 157 (1) (2010) A82–A97.
[26] H.A. Gasteiger, N.M. Markovic, Just a dream-or future reality? Science 324 (5923) (2009) 48–49.
[27] M. Oezaslan, P. Strasser, Activity of dealloyed $PtCO_3$ and $PtCu_3$ nanoparticle electrocatalyst for oxygen reduction reaction in polymer electrolyte membrane fuel cell, Journal of Power Sources 196 (2010) 5240–5249.
[28] H.T. Duong, et al., Oxygen reduction catalysis of the Pt_3CO alloy in alkaline and acidic media studied by X-ray photoelectron spectroscopy and electrochemical methods, Journal of Physical Chemistry C 111 (2007) 13460–13465.
[29] A.T. Hubbard, Personal Statement.
[30] A.T. Hubbard, E.Y. Cao, D.A. Stern, Surface-analysis of electrodes by ultra-high-vacuum techniques – acetonitrile solvent chemisorption at Pt(1 1 1), Electrochimica Acta 39 (8–9) (1994) 1007–1014.
[31] R.B. Kutz, et al., Reaction pathways of ethanol electrooxidation on polycrystalline platinum catalysts in acidic electrolytes, Journal of Catalysis 278 (2) (2011) 181–188.
[32] R.B. Kutz, et al., Study of ethanol electrooxidation in alkaline electrolytes with isotope labels and sum-frequency generation, Journal of Physical Chemistry Letters 2 (17) (2011) 2236–2240.
[33] L.R. Lynd, C.H.D. Cruz, Make way for ethanol, Science 330 (2010) 1176–1177.
[34] F. Colmati, et al., Surface structure effects on the electrochemical oxidation of ethanol on platinum single crystal electrodes, Faraday Discussions 140 (2008) 379–397.
[35] F. Vigier, et al., Electrocatalysis for the direct alcohol fuel cell, Topics in Catalysis 40 (1–4) (2006) 111–121.
[36] S. Rousseau, et al., Direct ethanol fuel cell (DEFC): electrical performances and reaction products distribution under operating conditions with different platinum-based anodes, Journal of Power Sources 158 (1) (2006) 18–24.
[37] F. Vigier, et al., On the mechanism of ethanol electro-oxidation on Pt and PtSn catalysts: electrochemical and in situ IR reflectance spectroscopy studies, Journal of Electroanalytical Chemistry 563 (1) (2004) 81–89.
[38] F. Vigier, et al., Development of anode catalysts for a direct ethanol fuel cell, Journal of Applied Electrochemistry 34 (4) (2004) 439–446.
[39] C. Lamy, et al., Recent progress in the direct ethanol fuel cell: development of new platinum–tin electrocatalysts, Electrochimica Acta 49 (22–23) (2004) 3901–3908.
[40] H. Hitmi, et al., A kinetic, analysis of the electrooxidation of ethanol at a platinum-electrode in acid-medium, Electrochimica Acta 39 (3) (1994) 407–415.
[41] M.C. Morin, et al., Structural effects in electrocatalysis – oxidation of ethanol on platinum single-crystal electrodes – effect of Ph, Journal of Electroanalytical Chemistry 283 (1–2) (1990) 287–302.
[42] J.M. Perez, et al., In situ infrared reflectance spectroscopic study of the early stages of ethanol adsorption at a platinum-electrode in acid-medium, Journal of Electroanalytical Chemistry 262 (1–2) (1989) 251–261.
[43] B. Beden, et al., Insitu analysis by infrared reflectance spectroscopy of the adsorbed species resulting from the electrosorption of ethanol on platinum in acid-medium, Journal of Electroanalytical Chemistry 229 (1–2) (1987) 353–366.
[44] C. Lamy, Electrocatalytic oxidation of organic compounds on noble metals in aqueous solution, Electrochimica Acta 29 (1984) 1581.
[45] C. Lamy, et al., Recent advances in the development of direct alcohol fuel cells (DAFC), Journal of Power Sources 105 (2) (2002) 283–296.
[46] H. Wang, Z. Jusys, R.J. Behm, Ethanol electrooxidation on a carbon-supported Pt catalyst: reaction kinetics and product yields, Journal of Physical Chemistry B 108 (50) (2004) 19413–19424.
[47] M. Heinen, Z. Jusys, R.J. Behm, Ethanol, acetaldehyde and acetic acid adsorption/electrooxidation on a Pt thin film electrode under continuous electrolyte flow: an in situ ATR-FTIRS flow cell study, Journal of Physical Chemistry C 114 (2010) 9850.
[48] X.D. Zhu, et al., Coverage dependence of surface optical 2nd-harmonic generation from CO/NI(1 1 0) – investigation with a nonlinear-interference technique, Physical Review Letters B 43 (1991) 11571.
[49] Y.R. Shen, Surface-properties probed by 2nd-harmonic and sum-frequency generation, Nature 337 (1989) 519–525.
[50] B. Braunschweig, et al., Sum-frequency generation of acetate adsorption on Au and Pt surfaces: molecular structure effects, Journal of Chemical Physics 133 (23) (2010) 8.
[51] G.Q. Lu, et al., Quantitative vibrational sum-frequency generation spectroscopy of thin layer electrochemistry: CO on a Pt electrode, Surface Science 585 (1) (2005) 3–16.
[52] A. Lagutchev, et al., Vibrational sum frequency generation studies of the $(2 \times 2) \rightarrow (\text{root } 19 \times \text{root } 19)$ phase transition of CO on Pt(1 1 1) electrodes, Journal of Chemical Physics 125 (2006) 154705.
[53] A.H.S. Lagutchev, D. Dlott, Nonresonant background suppression in broadband vibrational sum-frequency generation spectroscopy, Journal of Physical Chemistry C 111 (2007) 13645.
[54] A. Lagutchev, et al., Compact broadband vibrational sum-frequency generation spectrometer with nonresonant suppression, Spectrochimica Acta, Part A 75 (4) (2010) 1289–1296.
[55] R.L. Behrens, et al., Reaction pathways of ethanol electrooxidation on polycrystalline platinum catalysts in acidic electrolytes, Journal of Electroanalytical Chemistry 649 (2010) 32–36.
[56] B. Braunschweig, et al., Real-time investigations of Pt(1 1 1) surface transformations in sulfuric acid solutions, Journal of the American Chemical Society 132 (2010) 14036.
[57] A.B. Anderson, O-2 reduction and CO oxidation at the Pt-electrolyte interface. The role of H2O and OH adsorption bond strengths, Electrochimica Acta 47 (22–23) (2002) 3759–3763.
[58] A.B. Anderson, et al., Activation energies for oxygen reduction on platinum alloys: theory and experiment, Journal of Physical Chemistry B 109 (3) (2005) 1198–1203.
[59] J. Roques, A.B. Anderson, Electrode potential-dependent stages in OHads formation on the Pt3Cr alloy (1 1 1) surface, Journal of the Electrochemical Society 151 (11) (2004) E340–E347.
[60] E. Santos, W. Schmickler, Electronic interactions decreasing the activation barrier for the hydrogen electro-oxidation reaction, Electrochimica Acta 53 (21) (2008) 6149–6156.
[61] F. Wilhelm, et al., A model for proton transfer to metal electrodes, Journal of Physical Chemistry C 112 (29) (2008) 10814–10826.
[62] J.K. Nørskov, et al., Origin of the overpotential for oxygen reduction at a fuel-cell cathode, Journal of Physical Chemistry B 108 (46) (2004) 17886–17892.
[63] J.S. Filhol, M. Neurock, Elucidation of the electrochemical activation of water over Pd by first principles, Angewandte Chemie-International Edition 45 (3) (2006) 402–406.
[64] C.D. Taylor, et al., First principles reaction modeling of the electrochemical interface: consideration and calculation of a tunable surface potential from atomic and electronic structure, Physical Review B 73. (16) (2006).
[65] M. Otani, et al., Structure of the water/platinum interface – a first principles simulation under bias potential, Physical Chemistry Chemical Physics 10 (25) (2008) 3609–3612.
[66] R. Jinnouchi, A.B. Anderson, Electronic structure calculations of liquid–solid interfaces: combination of density functional theory and modified Poisson–Boltzmann theory, Physical Review B 77 (24) (2008).
[67] J. Rossmeisl, et al., Modeling the electrified solid–liquid interface, Chemical Physics Letters 466 (1–3) (2008) 68–71.
[68] G. Samjeske, A. Miki, M. Osawa, Electrocatalytic oxidation of formaldehyde on platinum under galvanostatic and potential sweep conditions studied by time-resolved surface-enhanced infrared spectroscopy, Journal of Physical Chemistry C 111 (41) (2007) 15074–15083.
[69] Y.X. Chen, et al., Formate, an active intermediate for direct oxidation of methanol on Pt electrode, Journal of the American Chemical Society 125 (13) (2003) 3680–3681.
[70] M. Neurock, M. Janik, A. Wieckowski, A first principles comparison of the mechanism and site requirements for the electrocatalytic oxidation of methanol and formic acid over Pt, Faraday Discussions 140 (2009) 363–378.
[71] D. Kardash, C. Korzeniewski, N. Markovic, Effects of thermal activation on the oxidation pathways of methanol at bulk Pt–Ru alloy electrodes, Journal of Electroanalytical Chemistry 500 (1–2) (2001) 518–523.
[72] N.M. Markovic, P.N. Ross, Surface science studies of model fuel cell electrocatalysts, Surface Science Reports 45 (4–6) (2002) 121–229.
[73] A.V. Tripkovic, et al., Methanol electrooxidation on supported Pt and PtRu catalysts in acid and alkaline solutions, Electrochimica Acta 47 (22–23) (2002) 3707–3714.
[74] F. Maillard, et al., Ru-decorated Pt surfaces as model fuel cell electrocatalysts for CO electrooxidation, Journal of Physical Chemistry B 109 (34) (2005) 16230–16243.
[75] T. Seiler, et al., Poisoning of PtRu/C catalysts in the anode of a direct methanol fuel cell: a DEMS study, Electrochimica Acta 49 (22–23) (2004) 3927–3936.

[76] K.A. Friedrich, et al., CO adsorption and oxidation on a Pt(1 1 1) electrode modified by ruthenium deposition: an IR spectroscopic study, Journal of Electroanalytical Chemistry 402 (1–2) (1996) 123–128.
[77] R. Ianniello, et al., Co adsorption and oxidation on Pt and Pt–Ru Alloys – dependence on substrate composition, Electrochimica Acta 39 (11–12) (1994) 1863–1869.
[78] C. Roth, et al., A Pt/Ru nanoparticulate model system to study the bifunctional mechanism of electrocatalysis, Journal of Electroanalytical Chemistry 581 (1) (2005) 79–85.
[79] O.A. Petrii, Pt–Ru electrocatalysts for fuel cells: a representative review, Journal of Solid State Electrochemistry 12 (5) (2008) 609–642.
[80] C. Lu, et al., UHV, electrochemical NMR, and electrochemical studies of platinum/ruthenium fuel cell catalysts, Journal of Physical Chemistry B 106 (37) (2002) 9581–9589.
[81] Y.Y. Tong, A. Wieckowski, E. Oldfield, NMR of electrocatalysts, Journal of Physical Chemistry B 106 (10) (2002) 2434–2446.
[82] Y.Y. Tong, et al., A detailed NMR-based model for CO on Pt catalysts in an electrochemical environment: Shifts, relaxation, back-bonding, and the Fermi-level local density of states, Journal of the American Chemical Society 122 (6) (2000) 1123–1129.
[83] Y.Y. Tong, et al., An NMR investigation of CO tolerance in a Pt/Ru fuel cell catalyst, Journal of the American Chemical Society 124 (2002) 468–473.
[84] F.B. de Mongeot, et al., CO adsorption and oxidation on bimetallic Pt/Ru(0 0 0 1) surfaces – a combined STM and TPD/TPR study, Surface Science 411 (3) (1998) 249–262.
[85] H.A. Gasteiger, et al., Electrooxidation of small organic molecules on well-characterized Pt–Ru alloys, Electrochimica Acta 39 (11–12) (1994) 1825–1832.
[86] N.M. Markovic, et al., Electrooxidation mechanism of methanol and formic acid on Pt–Ru alloy surfaces, Electrochimica Acta 40 (1) (1995) 91–98.
[87] S.R. Brankovic, et al., Electrosorption and catalytic properties of bare and Pt modified single crystal and nanostructured Ru surfaces, Journal of Electroanalytical Chemistry 524 (2002) 231–241.
[88] S.C.S. Lai, et al., Effects of electrolyte pH and composition on the ethanol electro-oxidation reaction, Catalysis Today 154 (1–2) (2010) 92–104.
[89] M. Neurock, First principles modeling for the electrooxidation of small molecules, in: W. Vielstich, H.A. Gasteiger, H. Yokokawa (Eds.), Handbook of Fuel Cells, J. Wiley & Sons, Weinheim, 2009.
[90] M. Janik, M. Neurock, Unpublished Results, 2008.
[91] S.C.S. Lai, et al., Effects of electrolyte pH and composition on the ethanol electro-oxidation reaction, Catalysis Today 154 (2010) 92–104.
[92] S.C.S. Lai, M.T.M. Koper, The influence of surface structure on selectivity in the ethanol electro-oxidation reaction on platinum, Journal of Physical Chemistry Letters 1 (7) (2010) 1122–1125.
[93] F. Li, D.D. Hibbitts, M. Neurock, Unpublished Results, 2012.
[94] H.W. Colmenares, et al., Electrochimica Acta 52 (2006) 221–233.
[95] F. Vigier, et al., Journal of Electroanalytical Chemistry 563 (2004) 81–89.
[96] K. Wang, et al., Electrochimica Acta 41 (16) (1996) 2587–2593.
[97] H. Wang, Z. Jusys, R.J. Behm, Journal of Power Sources 154 (2) (2006) 351–359.
[98] Q. Wang, et al., Physical Chemistry Chemical Physics 9 (21) (2007) 2686–2696.
[99] J. Rossmeisl, et al., Calculated phase diagrams for the electrochemical oxidation and reduction of water over Pt(1 1 1), Journal of Physical Chemistry B 110 (43) (2006) 21833–21839.
[100] S.C.S. Lai, M.T.M. Koper, Electro-oxidation of ethanol and acetaldehyde on platinum single-crystal electrodes, Faraday Discussions 140 (2008) 399–416.
[101] R.A. van Santen, M. Neurock, Theory of surface chemical reactivity, in: H.K.G. Ertl, J. Weitcamp (Eds.), Handbook of Catalysis, Springer Verlag, Inc., 1997, pp. 942–958.
[102] R.A. van Santen, M. Neurock, Molecular Heterogeneous Catalysis: A Mechanistic and Computational Approach, VCH-Wiley, Weinheim, 2006.
[103] R.A. van Santen, M. Neurock, S.G. Shetty, Reactivity theory of transition-metal surfaces: a Bronsted-Evans-Polanyi linear activation energy-free-energy analysis, Chemical Reviews 110 (4) (2010) 2005–2048.
[104] T. Bligaard, J.K. Nørskov, Ligand effects in heterogeneous catalysis and electrochemistry, Electrochimica Acta 52 (18) (2007) 5512–5516.
[105] J. Greeley, et al., Computational high-throughput screening of electrocatalytic materials for hydrogen evolution, Nature Materials 5 (11) (2006) 909–913.
[106] B.N. Zope, et al., Reactivity of the gold/water interface during selective oxidation catalysis, Science 330 (6000) (2010) 74–78.
[107] W.C. Ketchie, M. Murayama, R.J. Davis, Promotional effect of hydroxyl on the aqueous phase oxidation of carbon monoxide and glycerol over supported Au catalysts, Topics in Catalysis 44 (1–2) (2007) 307–317.
[108] Y. Kwon, S. Lai, P. Rodriguez, Electrocatalytic oxidation of alcohols on gold in alkaline media: base or gold catalysis? Journal of the American Chemical Society 133 (2011) 6914–6917.
[109] Y. Kwon, M.T.M. Koper, Combining voltammetry with HPLC: application to electro-oxidation of glycerol, Analytical Chemistry 82 (13) (2010) 5420–5424.
[110] Y. Kwon, K.J.P. Schouten, M.T.M. Koper, Mechanism of the catalytic oxidation of glycerol on polycrystalline gold and platinum electrodes, ChemCatChem 3 (2011) 1176–1185.
[111] M.A. Sanchez-Castillo, et al., Gold-nanotube membranes for the oxidation of CO at gas–water interfaces, Angewandte Chemie-International Edition 43 (9) (2004) 1140–1142.
[112] X. Qian, et al., Quasiatomic orbitals for ab initio tight-binding analysis, Physical Review B 78 (2008) 1–22.
[113] D.D. Hibbitts, M. Neurock, Influence of oxygen and alkalinity during selective oxidation of ethanol over Pd catalysts, Journal of Catalysis, submitted for publication.
[114] H.A. Gasteiger, et al., Activity benchmarks and requirements for Pt, Pt-alloy, and non-Pt oxygen reduction catalysts for PEMFCs, Applied Catalysis B: Environmental 56 (2005) 9–35.
[115] A. Damjanovic, V. Brusic, Electrode kinetics of oxygen reduction on oxide-free platinum electrodes, Electrochim Acta 12 (1967) 615–628.
[116] A. Damjanovic, D.B. Sepa, An analysis of the pH dependence of enthalpies and Gibbs energies of activation for O_2 reduction at Pt electrodes in acid solutions, Electrochimica Acta 35 (1990) 1157–1162.
[117] N. Markovic, Kinetics of oxygen reduction on Pt(h k l) electrodes: implications for the crystallite size effect with supported Pt electrocatalysts, Journal of the Electrochemical Society 144 (1997) 1591.
[118] N.M. Markovic, Surface science studies of model fuel cell electrocatalysts, Surface Science Reports 45 (2002) 117–229.
[119] M. Tsuda, H. Kasai, Proton transfer to oxygen adsorbed on Pt: how to initiate oxygen reduction reaction, Journal of the Physical Society of Japan 76 (2007) 024801.
[120] E. Yeager, Electrocatalysts for O_2 reduction, Electrochimica Acta 29 (1984) 1527–1537.
[121] M.J. Janik, C.D. Taylor, M. Neurock, First-principles analysis of the initial electroreduction steps of oxygen over Pt(1 1 1), Journal of the Electrochemical Society 156 (2009) B126.